

Observation of Strong Coupling between One Atom and a Monolithic Microresonator

Takao Aoki^a, Barak Dayan, E. Wilcut, W. P. Bowen^b, A. S. Parkins^c, and H. J. Kimble

Norman Bridge Laboratory of Physics 12-33, California Institute of Technology, Pasadena, California 91125, USA

T. J. Kippenberg^d and K. J. Vahala

T. J. Watson Laboratory of Applied Physics, California Institute of Technology, Pasadena, California 91125, USA

(Dated: November 26, 2024)

Over the past decade, strong interactions of light and matter at the single-photon level have enabled a wide set of scientific advances in quantum optics and quantum information science. This work has been performed principally within the setting of cavity quantum electrodynamics [1, 2, 3, 4] with diverse physical systems [5], including single atoms in Fabry-Perot resonators [1, 6], quantum dots coupled to micropillars and photonic bandgap cavities [7, 8], and Cooper-pairs interacting with superconducting resonators [9, 10]. Experiments with single, localized atoms have been at the forefront of these advances [11, 12, 13, 14, 15] with the use of optical resonators in high-finesse Fabry-Perot configurations [16]. As a result of the extreme technical challenges involved in further improving the multilayer dielectric mirror coatings [17] of these resonators and in scaling to large numbers of devices, there has been increased interest in the development of alternative microcavity systems [5]. Here we show strong coupling between individual Cesium atoms and the fields of a high-quality toroidal microresonator. From observations of transit events for single atoms falling through the resonator’s evanescent field, we determine the coherent coupling rate for interactions near the surface of the resonator. We develop a theoretical model to quantify our observations, demonstrating that strong coupling is achieved, with the rate of coherent coupling exceeding the dissipative rates of the atom and the cavity. Our work opens the way for investigations of optical processes with single atoms and photons in lithographically fabricated microresonators. Applications include the implementation of quantum networks [18, 19], scalable quantum logic with photons [20], and quantum information processing on atom chips [21].

The realization of large-scale quantum networks [18, 19] requires the capability to inter-connect many ‘quantum nodes’, each of which could consist of a microresonator containing a set of trapped atoms. The ‘quantum channels’ to connect these nodes would be optical fibres, with strong interactions in cavity quantum electrodynamics (QED) providing an efficient interface between light and matter. Here we provide a critical step towards a feasible quantum network by demonstrating strong coupling of single atoms to microresonators fabricated on Silicon wafers in large numbers by standard lithographic techniques followed by a laser-reflow process [22]. Combined with the capability to couple light efficiently to and from such cavities directly via a tapered optical fibre [23], toroidal microcavities offer promising capabilities for new nonlinear interactions of single atoms and photons across distributed networks.

Our efforts follow the pioneering work of V. Braginsky *et al.* [24] and later studies [25] by employing the whispering-gallery modes of fused silica microtoroidal resonators [26]. As depicted in Fig. 1, a Silicon chip containing a collection of 35 microtoroidal resonators is located inside a vacuum chamber at 10^{-9} Torr and is positioned to couple a particular resonator to a tapered fibre. The toroids have major diameter $D \simeq 44 \mu\text{m}$ and minor diameter $d \simeq 6 \mu\text{m}$ [26]. By judicious choice of the point of contact between the surface of the resonator and the tapered fibre, we attain critical coupling, in which the forward propagating power P_F in the fibre drops to near zero for the probe frequency ω_p equal to the cavity resonance frequency ω_C [23]. Measurements of the cavity transmission in the absence of atoms are presented in Fig. 2. Note that the forward flux P_F and associated transmission spectrum T_F are analogous to the reflected flux and reflection spectrum from a Fabry-Perot cavity [23]. By varying the temperature of the Silicon chip, the detuning $\Delta_{AC} \equiv \omega_C - \omega_A$ between ω_C and the atomic resonance at ω_A ($6S_{1/2}, F = 4 \rightarrow 6P_{3/2}, F' = 5'$ transition in Cesium) can be controlled with uncertainty $\simeq \pm 2$ MHz (see Appendix A).

Cold atoms are delivered to the vicinity of the toroidal resonator from a small cloud of Cesium atoms cooled to $T \simeq 10 \mu\text{K}$ and located 10 mm above the Silicon chip. Every 5 seconds, the cloud is dropped, resulting in about 2×10^6 atoms in a 3 mm ball at the height of the chip, with then a few dozen atoms passing through the external evanescent field of the toroidal resonator. By way of two single-photon detectors (D_{F1}, D_{F2}) (see Appendix A), we continuously monitor the forward propagating signal P_F from a frequency-stabilized probe beam P_{in} coupled to the toroidal resonator. The interaction of each individual atom with the evanescent field destroys the condition of critical coupling, leading to an increase in P_F . The measurement cycle then repeats itself for 2.5 seconds for a reference

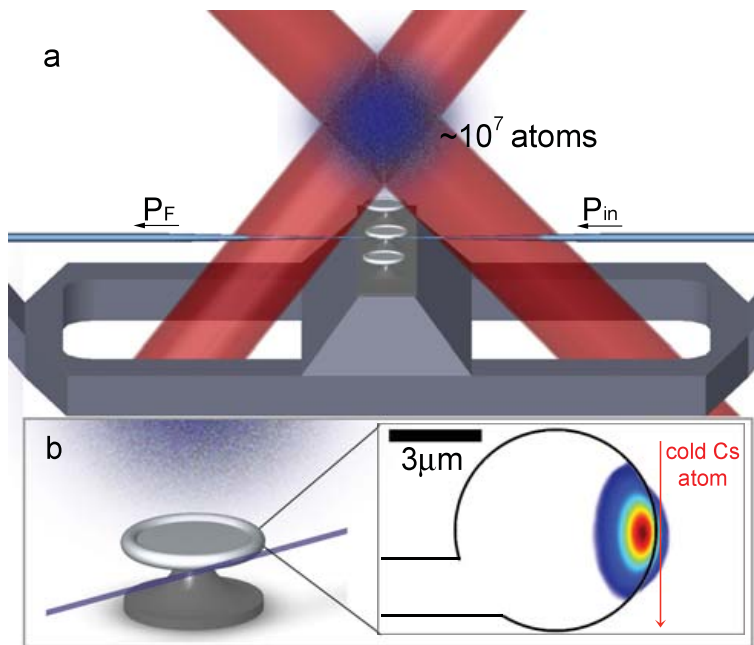


FIG. 1: **Simple diagram of the experiment.** (a) A cloud of cold Cesium atoms and associated trapping lasers above an array of microtoroidal resonators. Light from the probe beam P_{in} is coupled into a resonator by way of the fibre taper, with the forward propagating output P_F coupled out the taper. (b) Illustration of an SiO₂ microtoroidal resonator, fibre taper, and atom cloud above. The calculated field distribution for the lowest order resonator mode is shown by the color contour plot on the right. Cold Cesium atoms fall through the external evanescent field of this mode and are thereby strongly coupled to the resonator's field.

measurement, this time with no atomic cloud formed above the microtoroid.

Figure 3 displays typical records $C(t)$ for the number of single-photon detection events within time bins of $\delta t = 2 \mu s$ as functions of time t for the forward signal $P_F(t)$. Measurements are displayed with (Fig. 3(a)) and without (Fig. 3(b)) atoms for the case of equal probe and cavity frequencies, $\omega_p = \omega_C$, for $\Delta_{AC} \approx 0$, and with mean intracavity photon number $\bar{n}_0 \approx 0.3$ for the forward circulating mode of the toroidal resonator a (see Appendix A). The traces in both Fig. 3(a) and Fig. 3(b) exhibit background levels that result from the nonzero ratio $P_F/P_{in} \sim 0.005$ at critical coupling in the absence of atoms. However, Fig 3(a) clearly evidences sharp peaks of duration $\Delta t \approx 2 \mu s$ for the forward propagating light $P_F(t)$, with an individual peak shown more clearly in the inset. Each event arises from the transit of a single atom through the resonant mode of the microtoroid, with about 30 events per cycle observed. Fig. 3(c) examines the temporal profile of transit events in more detail by way of the cross correlation $\Gamma(\tau)$ of photoelectric counts $C_1(t_1), C_2(t_1 + \tau)$ from the detectors (D_{F1}, D_{F2}) for P_F (see Appendix A). This result agrees reasonably well with the theoretical prediction for atom transits through the calculated field distribution shown in Fig. 1(b).

By applying a threshold requiring $C(t) \geq 6$ counts for $C(t)$ as in Fig. 3(a, b), we find the average time dependence $\bar{C}_{\geq 6}(t)$ over about 100 measurement cycles. Fig. 3(d) displays the results both with and without atoms, with the average counts $\Sigma_6(t)$ derived from $\bar{C}_{\geq 6}(t)$ by summing over successive time bins $\delta t = 2 \mu s$ for 1 ms intervals. The peak in transit events is consistent with the expected distribution of arrival times for atoms dropped from our atom cloud. By contrast, negligible excess events (i.e., $C(t) \geq 6$) are recorded for the cases without atoms.

Focusing attention to the central region indicated by the dashed lines in Fig. 3(d), we examine in Fig. 3(e) the probability $P(C)$ to record C counts within $\delta t = 2 \mu s$. Evidently, when the atom cloud is present, there is a statistically significant increase (of at least fifteen sigma) in the number of events with $C \geq 4$. These are precisely the events illustrated by the inset in Fig. 3(a) and the cross correlation in Fig. 3(c), and are associated with single atom transits near the surface of the toroidal resonator. By varying the value of \bar{n}_0 , we have confirmed that the large transit events evident in Fig. 3 are markedly decreased for $\bar{n}_0 \gtrsim 1$ photon, which indicates the saturation of the atom-cavity system.

A quantitative description of our observations in Fig. 3 of individual atom transits requires the development of a new theoretical model in cavity QED. In the appendix, we present such a model and show that the underlying description of the interaction of an atom with the fields of the toroidal resonator is in terms of normal modes (A, B) (see Fig. 5 in Appendix B), which have mode functions $\psi_{A,B}(\rho, x, z)$ that are standing waves ($\cos kx, \sin kx$) around the circumference x of the toroid, with ρ the radial distance from the surface and z the vertical coordinate. $\psi_{A,B}(\rho, x, z)$

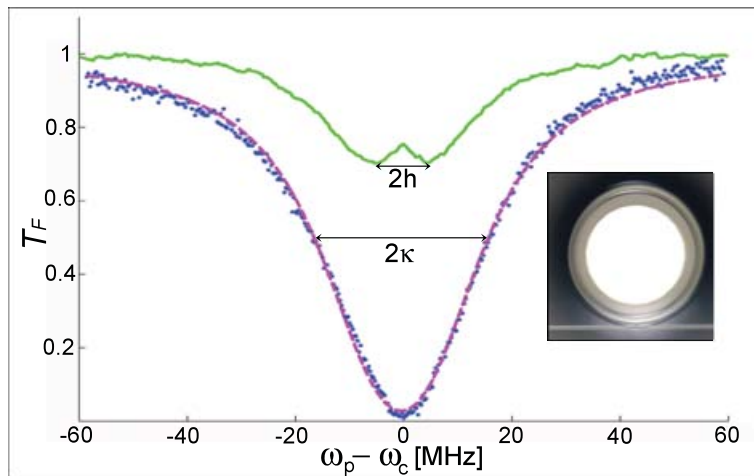


FIG. 2: **Cavity transmission function** $T_F = P_F/P_{in}$ **as a function of probe frequency** ω_p . The lower trace is taken for critical coupling, and the upper trace for conditions of under coupling [23]. From fits to such traces for critical coupling (red dashed curve), we find $(\kappa, h)/2\pi = (17.9 \pm 2.8, 4.9 \pm 1.3)$ MHz, with κ, h being the overall cavity field decay rate and the scattering-induced coupling between two counter-propagating modes of the microtoroid, respectively (see Appendix for more details). Inset – Photograph of a microtoroid and coupling fibre.

have a calculated peak coherent coupling $g_0/2\pi$ of 70 MHz for the lowest order modes of our resonator (such as that illustrated in Fig. 1(b)). The normal modes A,B result from the coupling of two oppositely directed travelling waves by scattering at rate h , with the resulting mode splitting manifest in Fig. 2. Note that the presence of two normal modes leads to a $\sqrt{2}$ increase in the coupling constant in our case as compared to the one predicted by the Jaynes-Cummings model for an atom interacting with a single traveling-wave mode (see Appendix B for further details).

Guided by this theory, we have performed a series of measurements similar to those presented in Fig. 3 to determine the coherent coupling rate g_0 for interactions of single atoms with our toroidal resonator, but now with various values of the atom-cavity detuning Δ_{AC} , keeping the probe resonant with the cavity: $\omega_p \approx \omega_C = \omega_A + \Delta_{AC}$. The qualitative idea is that large single-atom transit events will occur only over a range of detunings Δ_{AC} determined by g_0 . Specifically, the decrease in the forward transmission T_F induced by atom transits as a function of Δ_{AC} is described by a Lorentzian with width β set by g_0 (see Appendix B). In our case, $g_0 = g_0(\rho, x, z) \approx g_0(\rho, x, Vt)$, where V is the velocity of the dropped atoms in the z direction. Thus, a numerical integration was performed over ρ, x , and t to derive the theoretical expectation for $T_F(\Delta_{AC})$, presented in Fig. 4(a) for three values of g_0^m , where g_0^m is the maximal coupling that an atom can experience in its interaction with the cavity modes. Indeed, we see that the width β grows monotonically with g_0^m . However, the average value of T_F is not a parameter that is readily measured in our current experiment, in which we expect many short individual transits, some of which are too weak to be distinguished from the background noise (Fig. 3(e)). A parameter that describes our actual experimental measurements more closely is the probability to obtain a transit which results in transmission above a certain threshold. The two measures are closely related, such that this probability decreases with detuning Δ_{AC} in the same fashion as does T_F .

Figure 4(b-d) presents the results of our measurements for the average number of transit events per atom drop, $N_{drop}^{av}(C \geq C_0)$, which have photoelectric counts greater than or equal to a threshold value C_0 for a set of seven detunings Δ_{AC} . In accord with the expectation set by Fig. 4(a), there is a decrease in the occurrence of large transit events for increasing Δ_{AC} in correspondence to the decrease in the effective atom-cavity coupling coefficient for large atom-cavity detunings. The full curves shown in Fig. 4(b-d) are the results of theoretical calculation for these measurements, with the relevant cavity parameters (κ, h) determined from fits as in Fig. 2.

We first ask whether the data might be explained by an effective value g_0^e for the coherent coupling of atom and cavity field, without taking into account the fact that individual atoms transit at radial distances ρ which vary from atom to atom. Fig. 4(b) examines this possibility for various values of g_0^e , assuming a coupling coefficient $g_0^e \psi_{A,B}(x) = g_0^e [\cos kx, \sin kx]$ averaged along one period in x (as in Fig. 4(a)). Apparently, an effective value $g_0^e/2\pi \approx 40$ MHz provides reasonable correspondence between theory and experiment for large events $C \geq 6$.

We adapt our theory to the actual situation of atoms arriving randomly at radial and circumferential coordinates by introducing a mesh grid over (ρ, x) , and then computing the cavity transmission function $T_F(t)$ from $\psi_{A,B}(\rho, x, z(t))$ for atomic trajectories $z(t)$ over this grid. We account for the time resolution $\delta t = 2 \mu s$ of our data acquisition by a suitable average of $T_F(t)$ over such time bins (as was also true in Fig. 4(b)). The results from these calculations

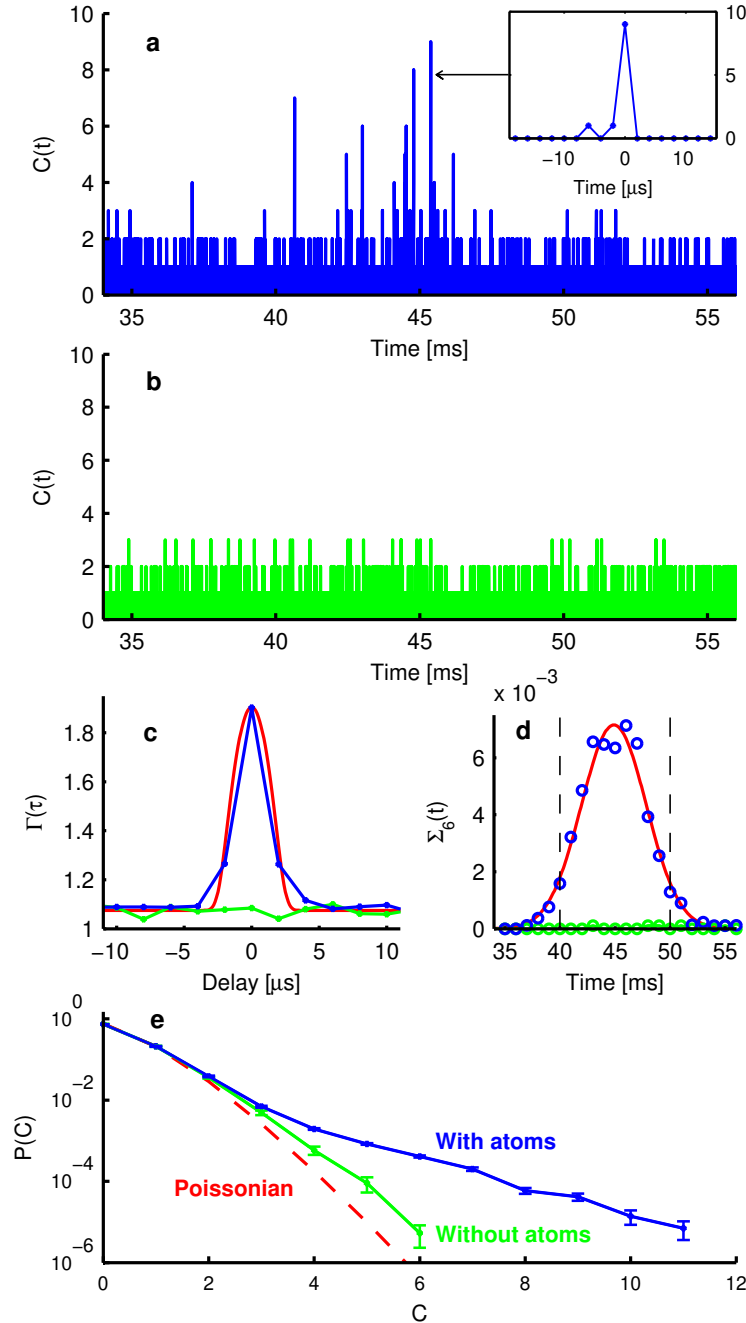


FIG. 3: Measurements of the forward signal P_F in the presence of falling atoms (blue) and without atoms (green). (a, b) Single-photon counting events $C(t)$ as a function of time t after the release of the cold atom cloud at $t = 0$, with (a) and without (b) atoms dropped. $C(t)$ gives the total number of counts recorded for time bins of $\delta t = 2 \mu\text{s}$ duration. The inset in (a) shows the time profile for a single-atom transit. (c) Normalized cross-correlation $\Gamma(\tau)$ of the forward signal counts from two detectors (D_{F1}, D_{F2}) showing the time profile associated with atom transit events. The smooth (red) curve is the theoretically predicted average cross correlation for a transit event with one atom, taking into account drop height of 10 mm and the spatial shape of the mode, as depicted in Fig. 1(b). (d) Counts $\Sigma_\delta(t)$ obtained from $\bar{C}_{\geq\delta}(t)$ by summing over 1 ms intervals, compared to a Gaussian distribution which fits the rate of atom transits assuming a 3 mm (FWHM) cloud of cold atoms dropped from 10 mm above the microtoroid. (e) Probability $P(C)$ to detect C counts within $\delta t = 2 \mu\text{s}$ bins for the central interval shown by the vertical dashed lines in (d), compared with Poissonian statistics (red) with the same mean number of counts (~ 0.25 per $2 \mu\text{s}$). The excess probability above the poissonian level in the no atoms case is predominately due to instability in the cavity temperature, which results in small fluctuations in the forward flux. Error bars show ± 1 s.d.

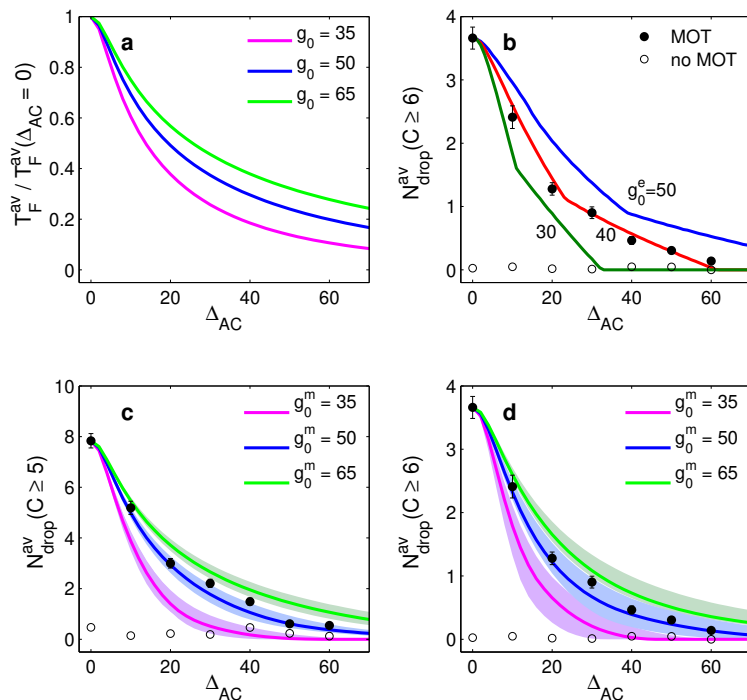


FIG. 4: **Measurements of transit events as a function of the atom-cavity detuning Δ_{AC} .** Events are shown in the presence of atoms (filled circles) and without atoms (empty circles), compared with the theoretical calculations (lines). **(a)** Theoretical calculation for the average of the transmission $T_F(\omega_p = \omega_C)$ as a function of (Δ_{AC}, g_0) . Red, $g_0=35$; blue, $g_0=50$; green, $g_0=65$. **(b-d)** Measurements for the average number of events per drop of the atom cloud $N_{drop}^{av}(C \geq C_0)$ plotted against the atom-cavity detuning Δ_{AC} , with $C_0 = 6$; **(b, d)** and $C_0 = 5$ **(c)**. Error bars show ± 1 s.d. The data are taken for probe frequency $\omega_p \approx \omega_C = \omega_A + \Delta_{AC}$. The full curves are theoretical results as discussed in the text. The widths of the curves are determined from the experimental uncertainties in (κ, h) . **(b)** Theory for $N_{drop}^{av}(C \geq 6)$ without radial averaging to deduce an effective coupling $g_0^e/2\pi = 40$ MHz. Theory for **(c)** $N_{drop}^{av}(C \geq 5)$ and **(d)** $N_{drop}^{av}(C \geq 6)$ with radial and azimuthal averaging leading to $g_0^m/2\pi = 50$ MHz. Red, $g_0^m=35$; blue, $g_0^m=50$; green, $g_0^m=65$.

are displayed in Fig. 4(c-d) as the set of full curves for three values of coherent coupling g_0 for the cavity mode functions $\psi_{A,B}(\rho, x, z)$, where in Fig. 4(b-d) the theory is scaled to match the measured $N_{drop}^{av}(C \geq C_0)$ at $\Delta_{AC} = 0$. From such comparisons, we determine the maximal accessible $g_0^m/2\pi = (50 \pm 12)$ MHz. Note that this conclusion is insensitive to the choice of cutoff C_0 over the range $4 \leq C_0 \leq 9$ for which we have significant transit events. Strong coupling with $g_0^m > (\kappa, \gamma)$ is thereby achieved, where $(\kappa, \gamma)/2\pi = (17.9 \pm 2.8, 2.6)$ MHz are the dissipative rates for the cavity field and the atom.

According to our calculations, $g_0^m/2\pi = 50$ MHz corresponds to the coupling rate expected at a distance of roughly 45 nm from the surface of the microtoroid. We estimate that due to the attractive van der Waals forces (see Ref [27]), atoms which enter the evanescent field with a distance $\rho \leq 45$ nm from the microtoroid are expected to strike its surface in less than 1 μ s, thus preventing such atoms from generating appreciable transit events in the transmission function T_F .

In summary, we report the first observation of strong coupling for single atoms interacting with an optical resonator other than a conventional Fabry-Perot cavity. The monolithic microtoroidal resonators [22] employed here have the capability of input-output coupling with small parasitic losses, with a demonstrated ideality of more than 99.97% [23]. Moreover, quality factors $Q = 4 \times 10^8$ have been realized at $\lambda = 1550$ nm [28] and $Q \simeq 10^8$ at $\lambda = 850$ nm [26], with good prospects for improvements to $Q \simeq 10^{10}$ [29]. For these parameters, the efficiency for coupling single photons into and out of the resonator could approach $\epsilon \sim 0.99 - 0.999$ [23], while still remaining firmly in the regime of strong coupling [26]. Such high efficiency is critical for the realization of scalable quantum networks [18, 19] and photonic quantum computation [20]. Indeed, of the diverse possibilities for the distribution and processing of quantum information with optical cavities [5, 7, 8], the system of single atoms coupled to microtoroidal resonators arguably provides one of the most promising avenues. Beyond efficient input-output coupling [23], strong coupling to a material system with long-lived internal states has now been achieved, although here in a primitive, proof-of-principle setting. An outstanding technical challenge is to trap single atoms near the surface of the microtoroid, with one possibility

having been investigated in ref. [30].

Acknowledgements – We thank M. Eichenfield, K. W. Goh and S. M. Spillane for their contributions to the early stages of this experiment, and T. Carmon, A. Gross and S. Walavalker for their contributions to the current realization. The work of H.J.K. is supported by the National Science Foundation, the Disruptive Technology Office of the Department of National Intelligence, the Army Research Office, and Caltech. The work of K.J.V. is supported by DARPA, the Caltech Lee Center and the National Science Foundation. B.D., W.P.B. and T.J.K. acknowledge support as Fellows of the Center for the Physics of Information at Caltech. E.W. acknowledges support as a Ford Predoctoral Fellow from the US National Academies. A.S.P. acknowledges support from the Marsden Fund of the Royal Society of New Zealand.

APPENDIX A: EXPERIMENTAL DETAILS

Preparation and characterization of cold atoms – Each measurement cycle in our experiment takes about 2.5 sec, and includes approximately 2 seconds for loading a magneto-optical trap (MOT), followed by 20 ms of polarization-gradient cooling of the atoms (with the magnetic fields for the MOT turned off). The trapping and cooling beams are then switched off and the atoms fall on the microtoroid.

For each run, we measure the number and arrival times of atoms in the falling atom cloud 2 mm above the microtoroid with a laser beam resonant with the $6S_{1/2}, F = 4 \rightarrow 6P_{3/2}, F' = 4'$ transition [31]. In each cycle we observe approximately 30 atom transits during the center 10 ms of our data-collection time window. This value is in a reasonable agreement with the theoretically calculated rate of 20 transits, which was derived by comparing the measured density of the falling atom cloud to the numerically calculated interaction area of the evanescent field. Every cycle with cold atoms is followed by an identical cycle with no trapped atoms for which the magnetic field for the MOT is turned off during the loading period. We also carried out other tests for the “no atoms” case, including switching off the repumping light for the MOT (with all other parameters unchanged).

Excitation and detection system – The frequency ω_p of the probe beam P_{in} in Fig. 1(a) is actively stabilized to a fixed detuning from the atomic resonance $\Delta_A = \omega_A - \omega_p$ via saturation spectroscopy to within ± 100 kHz. The cavity resonance at ω_C is monitored relative to ω_A and ω_p for each drop of the atom cloud and each reference cycle, and is controlled by temperature-tuning a thermoelectric device upon which the Silicon chip is mounted, with a frequency shift of approximately 3 MHz per mK of temperature change. Data is automatically recorded whenever the condition of critical coupling (i.e. $P_F < 1\%$ of the maximal value of 30 counts per $2 \mu s$) was achieved, corresponding to $\omega_p = \omega_C$ to within ± 2 MHz. Note that in our experiment we use blue detuning of the cavity and the probe relative to the atom, since red detuning could lead to a resonant interaction with the $6S_{1/2} F=4 \rightarrow 6P_{3/2} F' = 4'$ transition at large atom-cavity detuning $\Delta_{AC} \equiv \omega_C - \omega_A$. Additionally, blue detuning leads to an under-estimation of g , as the dipole forces become increasingly repulsive as we blue-detune our cavity, possibly leading to a more rapid reduction in the probability of transits. However, our calculations indicate that in our current experimental settings the light forces are significantly smaller than the van der Waals forces over the entire relevant interaction region of the atom with the evanescent field, and their effect on the atom’s motion and temperature is small. This situation is mostly due to the small populations of the dressed states that are coupled to the atom for excitation with $\omega_p \approx \omega_C$. Specifically, in our experiment the probe field frequency is always tuned to the empty cavity resonance, between the two vacuum-Rabi sidebands which correspond to the two dressed states of the atom and the coupled cavity mode (as described in Fig. 5). Thus, as the energy splitting between these states (and hence the associated dipole potential) grows during the atom transit, their population drops dramatically (and so does their contribution to the mechanical potential experienced by the atom), as they decouple from the probe field, leading to the described increase in the forward flux T_F . The resulting forces are of the order of few MHz/ μm , leading to estimated displacements of up to 40 nm during the $2 \mu s$ of atom transit for intermediate values of Δ_{AC} . Further measurements to explore the effect of light forces along with its inclusion in the theoretical model are in progress.

The probe P_{in} enters the vacuum apparatus by way of a single-mode fibre through a Teflon feedthrough [32]. This fibre is spliced to the fibre taper. The forward propagating signal P_F in Fig. 1(a) exits the vacuum chamber in the same fashion. P_F is then directed to a 50:50 fibre beam splitter whose outputs are detected by a pair of single-photon counting modules (SPCMs) (D_{F1}, D_{F2}) each with overall quantum efficiency $\alpha \simeq 0.5$ and dark counts < 100 per second. Using two detectors enables us to avoid, or at least assess, phenomena that are related to the non-ideality of these detectors, such as their ~ 50 ns dead time, saturation at fluxes exceeding a few million counts per second, “after-pulsing” effects which may result in a false second count, etc. The two detectors allow the detection of photons that are separated temporally by less than the dead time of these detectors (which are not number-resolving), and increase the maximal flux of photons that can be detected by our system before saturation effects take place. This method also enables further analysis of the photon statistics of the light, such as the cross-correlation between the two series of photon counts presented in Fig. 3(c).

Detection events from (D_{F1}, D_{F2}) are time-stamped relative to the drop time of the atom cloud, and stored for later analysis. The data in the figures refers to the total counts from the combined outputs of (D_{F1}, D_{F2}) . The overall propagation efficiency ξ from the fibre taper at the position of the toroidal resonator to the input beam splitter for (D_{F1}, D_{F2}) is $\xi = 0.70 \pm 0.02$. An additional SPCM was used to monitor the backwards flux, namely light that was coupled into the cavity, scattered into the counter-propagating mode and then transmitted backwards into the taper. When atom transits occurred, the observed increase in the forward flux was accompanied by a decrease in this backward flux.

In the absence of an atom, the average intracavity photon number is $\bar{n}_0 \simeq 0.3$ for the forward propagating mode (a) for critical coupling at $\omega_p = \omega_C$. If the probe is then detuned such that $|\omega_p - \omega_C| \gg \kappa$, the average number of counts recorded in a $2 \mu\text{s}$ interval is $C_{\Delta \gg \kappa} \approx 30$, which provides a calibration of the flux P_F given the known propagation and detection losses.

APPENDIX B: THEORY FOR A TWO-LEVEL ATOM COUPLED TO TWO TOROIDAL MODES

To understand our observations in quantitative terms, we have developed a theoretical model for a two-level atom interacting with the quantized fields of the toroidal resonator. The two-level atom has transition frequency ω_A and raising and lowering operators σ^\pm . The two counter-propagating modes of the toroidal resonator are taken to be degenerate with common frequency ω_C (in the absence of scattering), and are described by annihilation (creation) operators a (a^\dagger) and b (b^\dagger), respectively. In our actual resonators, modes are coupled due to scattering with a strength that is parameterized by h . A coherent probe of frequency ω_p in the input field of the fibre taper, a_{in} , couples to mode a with a strength \mathcal{E}_p . The input field to mode b is taken to be vacuum as in our experiments. In a frame rotating at the probe frequency ω_p , a simple Hamiltonian that models our system is thus [33]

$$\begin{aligned} H/\hbar = & \Delta_A \sigma^+ \sigma^- + \Delta (a^\dagger a + b^\dagger b) + h (a^\dagger b + b^\dagger a) \\ & + (g_{\text{tw}}^* a^\dagger \sigma^- + g_{\text{tw}} \sigma^+ a) + (g_{\text{tw}} b^\dagger \sigma^- + g_{\text{tw}}^* \sigma^+ b) \\ & + (\mathcal{E}_p^* a + \mathcal{E}_p a^\dagger), \end{aligned} \quad (\text{B1})$$

where $\Delta_A = \omega_A - \omega_p$, $\Delta = \omega_C - \omega_p$. The coherent interaction of the atom with the evanescent traveling-wave fields of the a, b modes is described by $g_{\text{tw}} = g_0^{\text{tw}} \phi_{\text{tw}}^\pm(\rho, x, z)$, where the mode functions $\phi_{\text{tw}}^\pm(\rho, x, z) = f(\rho, z) e^{\pm ikx}$ with $f(\rho, z) \sim e^{-\alpha\rho}$ ($\alpha \sim 1/\lambda$). The coordinates (ρ, x, z) are derived from cylindrical coordinates (r, θ, z) , where r is the radial distance from the axis of symmetry of the toroid, with then $\rho = r - D/2$; θ is the azimuthal angle in a plane perpendicular to the symmetry axis, with $x = r\theta$ as the position around the circumference of the toroid; and z is the vertical dimension along the symmetry axis. k is the vacuum wave vector. The field decay rate for the resonator modes is $\kappa = \kappa_i + \kappa_{\text{ex}}$, where κ_i represents intrinsic losses and κ_{ex} describes extrinsic loss due to (adjustable) coupling of the modes to the fibre taper [23, 34, 35]. The atomic excited state population decays with rate 2γ .

The output field in the forward direction is given by $a_{\text{out}} = a_{\text{in}} + \sqrt{2\kappa_{\text{ex}}} a$ [36]. Assuming only weak excitation of the atom, we can compute the output photon flux from this relationship and a linearized approximation to the equations of motion for the atomic coherence $\langle \sigma^- \rangle$ and field amplitudes $\langle a \rangle$ and $\langle b \rangle$. Characteristic spectra $T_F(\omega_p)$ of the forward flux P_F as a function of probe detuning and for different x -coordinates of the atom are shown in Fig. 5, where $|g_{\text{tw}}|/2\pi = 70/\sqrt{2}$ MHz and $\Delta_{\text{AC}} = 0$. The spectra are normalized by the flux of a far-off-resonant probe field. Also shown is the spectrum in the absence of an atom ($g_{\text{tw}} = 0$), under the (experimental) conditions of critical coupling; specifically, where $\kappa_{\text{ex}} = \kappa_{\text{ex}}^{\text{cr}} = \sqrt{\kappa_i^2 + \hbar^2}$, for which $P_F(\Delta = 0) \approx 0$ [23, 34, 35].

The coupled-atom spectra shown in Fig. 5 can be understood by considering the normal modes of the microtoroidal resonator, $A = (a + b)/\sqrt{2}$ and $B = (a - b)/\sqrt{2}$, in terms of which the Hamiltonian can be written

$$\begin{aligned} H = & \Delta_A \sigma^+ \sigma^- + (\Delta + h) A^\dagger A + (\Delta - h) B^\dagger B \\ & + \frac{1}{\sqrt{2}} [\mathcal{E}_p^* (A + B) + \mathcal{E}_p (A^\dagger + B^\dagger)] \\ & + g_A (A^\dagger \sigma^- + \sigma^+ A) \\ & - i g_B (B^\dagger \sigma^- - \sigma^+ B). \end{aligned} \quad (\text{B2})$$

The coherent coupling for the (A, B) modes is given here by $g_{A,B} = g_0 \psi_{A,B}(\rho, x, z)$, where $g_0 = \sqrt{2} g_0^{\text{tw}}$. The mode functions $\psi_{A,B}(\rho, x, z)$ for the normal modes of the cavity are $\psi_A(\rho, x, z) = f(\rho, z) \cos(kx)$ and $\psi_B(\rho, x, z) = f(\rho, z) \sin(kx)$. Significantly, the underlying description of the interaction of an atom with the toroidal resonator is thus in terms of standing waves $\psi_{A,B}(\rho, x, z)$ along the surface of the toroid. The splitting for the normal modes (A, B) induced by scattering h is displayed for undercoupling to our resonator in Fig. 2.

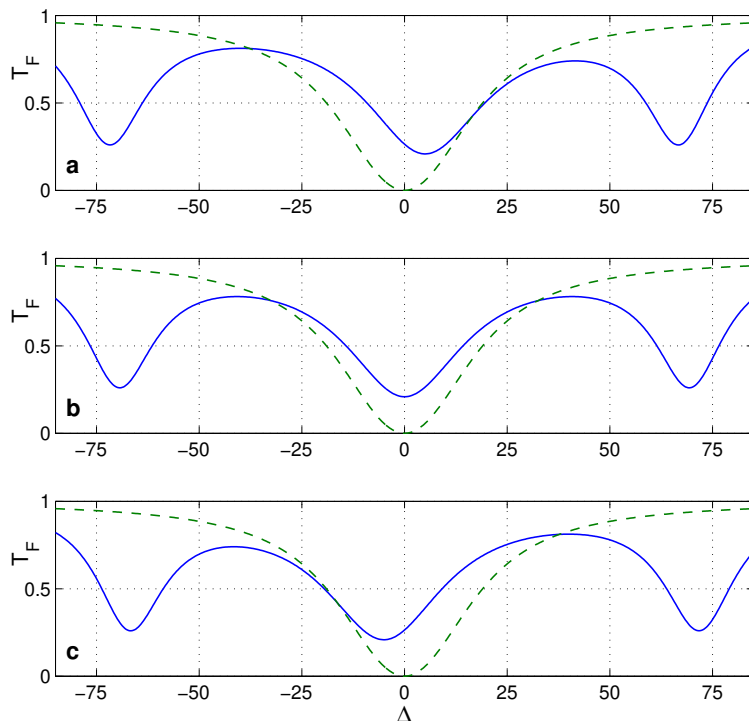


FIG. 5: Calculated spectra T_F of the forward flux in the presence of an atom (solid blue line) as a function of probe detuning Δ for different x -coordinates around the circumference of the toroid, namely (a) $kx = 0$, (b) $kx = \pi/4$, (c) $kx = \pi/2$. In all cases, $\Delta_{AC} = 0$ and $g_0/2\pi = 70$ MHz as appropriate for an atom at the external surface of our toroid. Also shown as the dashed curve is the spectrum in the absence of an atom ($g_0 = 0$) under the same conditions of critical coupling. $T_F(\omega_p)$ is normalized by the probe flux far off resonance, with (κ, h) determined from fits as in Fig. 2.

With reference to Fig. 5(a,c), we see that for $kx = 0$ ($\pi/2$) the atom couples only to mode A (B) of frequency $\omega_C + h$ ($\omega_C - h$) with strength g_0 , leading to a pronounced reduction in T_F at probe detunings $\Delta \simeq -h \pm g_0$ ($h \pm g_0$) for the case $\Delta_{AC} = 0$ shown, i.e., at the “vacuum-Rabi sidebands”. The central feature in the transmission spectrum T_F at $\Delta = h$ ($-h$) is the spectrum of the uncoupled normal mode B (A). By contrast, at $kx = \pi/4$ in (b), the atom couples with equal strength to both normal modes and a system of three coupled oscillators is realized (in the linear approximation), the normal mode frequencies of which occur at ω_C and $\sim (\omega_C \pm g_0)$ for $\Delta_{AC} = 0$.

The eigenvalues of the atom-toroid coupled system are drawn in Fig. 6(A) relative to the cavity resonance (blue, dashed), using the same parameters as Fig 5(b). In this representation the atom (red, dashed) has positive energy detuning for negative values of Δ_{AC} , and negative detuning for positive values of Δ_{AC} . The coupling with the atom lifts the degeneracy between the atom and the cavity at Δ_{AC} , leading to the expected splitting of $2g$ between dressed states #1 and #2. However, since the atom is never fully coupled to both normal modes (A,B), a third dressed state (#3, green) remains practically unchanged by the atom. This three mode structure is represented in both Fig. 5(a-c) and Fig. 6(B), which illustrate the transmission T_F at fixed $\Delta_{AC} = 0$ as a function of the probe frequency, demonstrating minima at 0 and $\pm g$. Similarly, the coupling strength manifests itself in the dependence of T_F on Δ_{AC} , as shown in Fig 6(C) for probe frequency fixed to the cavity resonance, as is the case in our experiment. Thus, the decrease in the forward flux T_F at the cavity resonance $\omega_p = \omega_C$ as a function of the cavity-atom detuning Δ_{AC} is a generic feature of the eigenvalue structure of the system.

Explicitly, under conditions of critical coupling, T_F can be expressed as

$$T_F|_{\omega_p=\omega_C} = \frac{4\kappa_i^2 |g_{tw}|^4 + h^2 (g_{tw}^2 + (g_{tw}^*)^2)^2}{\left[\gamma (h^2 + \kappa^2) + 2\kappa |g_{tw}|^2 \right]^2 + [\Delta_{AC} (h^2 + \kappa^2) - h (g_{tw}^2 + (g_{tw}^*)^2)]^2}. \quad (\text{B3})$$

This is simply a Lorentzian centered at

$$\Delta_{AC}^{center} = \frac{h}{h^2 + \kappa^2} (g_{tw}^2 + (g_{tw}^*)^2), \quad (\text{B4})$$

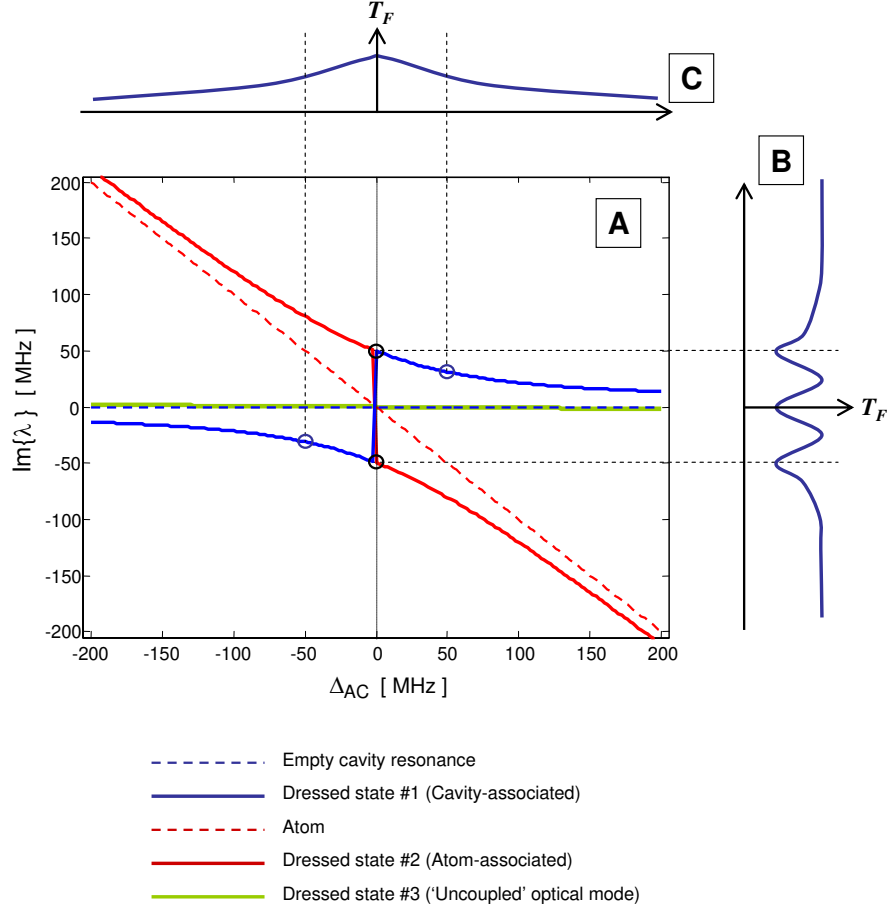


FIG. 6: (A) The three calculated eigenvalues of atom-toroid coupled system for $(g, \kappa, h) = (50, 18, 5)$ MHz. (B,C) Qualitative illustrations of the transmission T_F , (B) at fixed atom-cavity detuning $\Delta_{AC} = 0$ as a function of the probe frequency ω_p , and (C) as a function of Δ_{AC} , with probe frequency fixed to be $\omega_p = \omega_C$.

(note that when averaged over the azimuthal coordinate x , Δ_{AC}^{center} approaches zero), and with half-width

$$\beta = \gamma + \frac{2\kappa |g_{tw}|^2 + h (g_{tw}^2 + (g_{tw}^*)^2)}{h^2 + \kappa^2} \simeq \frac{2 |g_{tw}|^2}{\kappa} = \frac{|g_0|^2}{\kappa}, \quad (\text{B5})$$

assuming $2|g_{tw}|^2/\kappa \gg \gamma$ and $h/\kappa \ll 1$. The above result for T_F , averaged over the azimuthal coordinate x , is shown in Fig. 7 as a function of Δ_{AC} and $g_0 = \sqrt{2} g_{tw}$. Note that the half-widths of the curves $T_F(\Delta_{AC})$ are well-approximated by g_0^2/κ . Radial and temporal averaging leads to substantial narrowing of the curves $T_F(\Delta_{AC})$, producing a $\beta_{\text{effective}}$ which, while significantly smaller than the β defined in Eq. (5), maintains the dependence on the maximum coupling strength g_0^m , as illustrated in Fig. 4. Therefore, given knowledge of κ and γ , a measurement of the dependence of T_F on Δ_{AC} yields g_0 directly.

Note that the linear model presented here is adequate for the regime of our current experiment, as we have confirmed by numerical solutions of the full master equation. For the probe resonant with the cavity frequency, $\omega_p = \omega_C$, the population in the atomic excited state remains negligible for the conditions of our experiment.

It is interesting to contrast our model and the conventional Jaynes-Cummings model, which considers a two-level system coupled to only one electromagnetic field mode (for a given polarization), as is typically the case with Fabry-Perot resonators. As described above, unlike the two dressed states of the Jaynes-Cummings model, there are three eigenstates in our case. In the specific cases of $kx = 0, \pi/2$, two dressed states correspond to the vacuum-Rabi sidebands resulting from the coupling of the atom to one normal mode, while the third is essentially the normal mode that remains uncoupled with the atom. In principle, given that the coupling to the atom is stronger than the

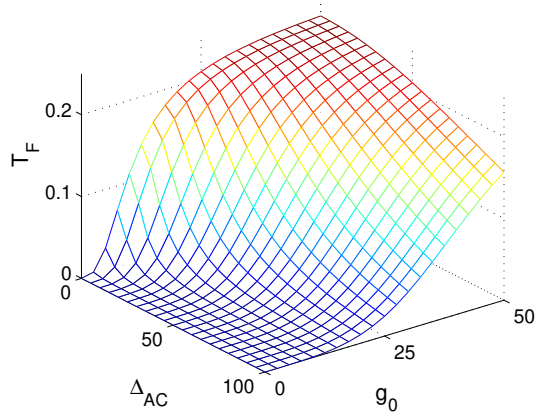


FIG. 7: Theoretical calculation for transmission $T_F(\omega_p = \omega_C)$ as a function of (Δ_{AC}, g_0) , with (κ_i, h) determined from fits to experimental data.

intermode coupling h , the definition of the normal modes could be chosen so the atom is at the node of one, and at the anti-node of the other for every value of kx . Thus, unlike the situation with Fabry-Perot resonators, where the atom could experience strong coupling at the anti-nodes of the standing wave and remain uncoupled to the cavity at the nodes of the standing wave, here the atom always obtains roughly the same degree of coupling with the cavity (either through one mode, the other or both). Accordingly, roughly half of the light in the cavity always remains uncoupled to the atom, leading to the third eigenvalue around zero detuning, as described in Fig 5. Note also that the presence of the atom redistributes the intensity between the two normal modes [37]. Finally, the existence of two normal modes leads to the factor of $\sqrt{2}$ between the coupling constant in our case and the one predicted by the Jaynes-Cummings model for a traveling wave $g_0 = \sqrt{2}g_0^{\text{tw}}$. Note that for the single-mode Janes-Cummings model, Eq. (B3) takes the form

$$T_F = \frac{\left(|g_{\text{tw}}|^2 / \kappa\right)^2}{\left(\gamma + |g_{\text{tw}}|^2 / \kappa\right)^2 + \Delta_{AC}^2}, \quad (\text{B6})$$

illustrating the same Lorentzian dependence on Δ_{AC} , with half-width $\beta_{\text{JC}} \sim |g_{\text{tw}}|^2 / \kappa$ for $|g_{\text{tw}}|^2 / \kappa \gg \gamma$.

APPENDIX C: CALCULATION OF THE COHERENT COUPLING PARAMETER g_0

For our particular toroidal resonator with major diameter $D \simeq 44 \mu\text{m}$ and minor diameter $d \simeq 6 \mu\text{m}$, we find numerically the lowest order traveling-wave mode functions $\phi_{\text{tw}}^{\pm}(\rho, x, z)$ of the resonator [26], from which follows the coupling parameters g_0^{tw} and g_0 . For the $6S_{1/2}, F = 4, m_F = 4 \rightarrow 6P_{3/2}, F' = 5', m_F' = 5'$ transition of the D_2 line of atomic Cesium, we find $g_0^{\text{tw}}/2\pi = 80 \text{ MHz}$ and thus $g_0/2\pi = \sqrt{2} \times 80 \text{ MHz}$. However, a circularly polarized field is required for coupling to this transition while the toroidal resonator supports linear polarization. Hence, for atoms uniformly distributed over the set of Zeeman states $\{m_F\}$ in the $F = 4$ ground state, we calculate g_0 from an average over Clebsch-Gordon coefficients for $\Delta m_F = 0$ transitions for $6S_{1/2}, F = 4 \leftrightarrow 6P_{3/2}, F' = 5'$, leading to $g_0/2\pi = 70 \text{ MHz}$, which is the value utilized in Fig. 5 above and quoted in the main text.

Current addresses –

^a TA – Department of Applied Physics, The University of Tokyo, Tokyo, Japan

^b WPB – Physics Department, University of Otago, Dunedin, New Zealand

^c ASP – Department of Physics, University of Auckland, Auckland, New Zealand

^d TJK – Max Planck Institute of Quantum Optics, Garching, Germany

-
- [1] R. Miller, T. E. Northup, K. M. Birnbaum, A. Boca, A. D. Boozer, and H. J. Kimble, “Trapped atoms in cavity QED: coupling quantized light and matter” *J. Phys. B: At. Mol. Opt. Phys.* **38**, S551-S565 (2005).
- [2] *Cavity Quantum Electrodynamics*, ed. P. Berman (San Diego: Academic Press, 1994).
- [3] H. Walther, “Quantum optics of single atoms” *Fortschr. Phys.* **52**, 1154-1165 (2004).
- [4] J. M. Raimond, T. Meunier, P. Bertet, S. Gleyzes, P. Maioli, A. Auffeves, G. Nogues, M. Brune, and S. Haroche, “Probing a quantum field in a photon box” *J. Phys. B: At. Mol. Opt. Phys.* **38**, S535-S550 (2005).
- [5] K. J. Vahala, “Optical microcavities” *Nature* **424**, 839-846 (2004) and references therein.
- [6] S. Nussmann, K. Murr, M. Hijlkema, B. Weber, A. Kuhn, and G. Rempe, “Vacuum-stimulated cooling of single atoms in three dimensions” *Nature Physics* **1**, 122 (2005).
- [7] G. Khitrova, H. M. Gibbs, M. Kira, S. W. Koch, and A. Scherer, “Vacuum Rabi splitting in semiconductors” *Nature Physics* **2**, 81-90 (2006), and references therein.
- [8] A. Badolato, K. Hennessy, M. Atature, J. Dreiser, E. Hu, P. M. Petroff, A. Imamoglu, “Deterministic Coupling of Single Quantum Dots to Single Nanocavity Modes” *Science* **308**, 1158-1161 (2005).
- [9] A. Wallraff, D. I. Schuster, A. Blais, L. Frunzio, R. S. Huang, J. Majer, S. Kumar, S. M. Girvin, and R. J. Schoelkopf, “Strong coupling of a single photon to a superconducting qubit using circuit quantum electrodynamics” *Nature* **431**, 162-167 (2004).
- [10] I. Chiorescu, P. Bertet, K. Semba, Y. Nakamura, C. J. P. M. Harmans, and J. E. Mooij “Coherent dynamics of a flux qubit coupled to a harmonic oscillator” *Nature* **431**, 159-162 (2004).
- [11] J. McKeever, A. Boca, A. D. Boozer, J. R. Buck, and H. J. Kimble, “Experimental realization of a one-atom laser in the regime of strong coupling” *Nature* **425**, 268-271 (2003).
- [12] J. McKeever, A. Boca, A. D. Boozer, R. Miller, J. R. Buck, A. Kuzmich, and H. J. Kimble, “Deterministic Generation of Single Photons from One Atom Trapped in a Cavity” *Science* **303**, 1992-1994 (2004).
- [13] M. Keller, B. Lange, K. Hayasaka, W. Lange, and H. Walther, “Continuous generation of single photons with controlled waveform in an ion-trap cavity system” *Nature* **431**, 1075-1078 (2004).
- [14] K. M. Birnbaum, A. Boca, R. Miller, A. D. Boozer, T. E. Northup, and H. J. Kimble, “Photon blockade in an optical cavity with one trapped atom” *Nature* **436**, 87-90 (2005).
- [15] T. Legero, T. Wilk, M. Hennrich, G. Rempe, and A. Kuhn, “Quantum Beat of Two Single Photons” *Phys. Rev. Lett.* **93**, 070503 (2004).
- [16] G. Rempe, R. J. Thompson, H. J. Kimble, and R. Lalezari, “Measurement of ultralow losses in an optical interferometer” *Opt. Lett.* **17**, 363-365 (1992).
- [17] C. J. Hood, J. Ye, and H. J. Kimble, “Characterization of high-finesse mirrors: Loss, Phase shifts, and mode structure in an optical cavity” *Phys. Rev. A* **64**, 033804 (2001).
- [18] J. I. Cirac, P. Zoller, H. J. Kimble, and H. Mabuchi, “Quantum State Transfer and Entanglement Distribution among Distant Nodes in a Quantum Network” *Phys. Rev. Lett.* **78**, 3221-3224 (1997).
- [19] H.-J. Briegel *et al.*, in *The Physics of Quantum Information*, edited by D. Bouwmeester, A. Ekert and A. Zeilinger, p. 192.
- [20] L.-M. Duan and H. J. Kimble, “Scalable Photonic Quantum Computation through Cavity-Assisted Interactions” *Phys. Rev. Lett.* **92**, 127902 (2004).
- [21] P. Treutlein, T. Steinmetz, Y. Colombe, P. Hommelhoff, J. Reichel, M. Greiner, O. Mandel, A. Widera, T. Rom, I. Bloch, T. W. Hänsch, “Quantum Information Processing Optical Lattices and Magnetic Microtraps” quant-ph/0605163.
- [22] D. K. Armani, T. J. Kippenberg, S. M. Spillane, and K. J. Vahala, “Ultra-high-Q toroid microcavity on a chip” *Nature* **421**, 925-928 (2003).
- [23] S. M. Spillane, T. J. Kippenberg, O. J. Painter, and K. J. Vahala, “Ideality in a Fiber-Taper-Coupled Microresonator System for Application to Cavity Quantum Electrodynamics” *Phys. Rev. Lett.* **91**, 043902 (2003).
- [24] V. B. Braginsky, M. L. Gorodetsky, and V. S. Ilchenko, “Quality-factor and nonlinear properties of optical whispering-gallery modes” *Phys. Lett. A* **137**, 393-397 (1989).
- [25] D. W. Vernooy, A. Furusawa, N. Ph. Georgiades, V. S. Ilchenko, and H. J. Kimble, “Cavity QED with high-Q whispering gallery modes” *Phys. Rev. A* **57**, R2293-R2296 (1998).
- [26] S. M. Spillane, T. J. Kippenberg, K. J. Vahala, K. W. Goh, E. Wilcut, and H. J. Kimble, “Ultrahigh-Q toroidal microresonators for cavity quantum electrodynamics” *Phys. Rev. A* **71**, 013817 (2005).
- [27] J.-Y. Courtois, J.-M. Courty, J. C. Mertz, “Internal dynamics of multilevel atoms near a vacuum-dielectric interface” *Phys. Rev. A* **53**, 1862-1878 (1996).
- [28] T. J. Kippenberg, S. M. Spillane, and K. J. Vahala, “Demonstration of ultra-high-Q small mode volume toroid microcavities on a chip” *Apl. Phys. Lett.* **85**, 6113-6115 (2004).

- [29] D. W. Vernooy, V. S. Ilchenko, H. Mabuchi, E. W. Streed, and H. J. Kimble, “High-Q measurements of fused-silica microspheres in the near infrared” *Opt. Lett.* **23**, 247-249 (1998).
- [30] D. W. Vernooy and H. J. Kimble, “Quantum structure and dynamics for atom galleries” *Phys. Rev. A* **55**, 1239-1261 (1997).
- [31] Ying-Cheng Chen, Yean-An Liao, Long Hsu, and Ite A. Yu, “Simple technique for directly and accurately measuring the number of atoms in a magneto-optical trap” *Phys. Rev. A* **64**, 031401(R) (2001).
- [32] E. R. I. Abraham and E. A. Cornell, “Teflon feedthrough for coupling optical fibers into ultrahigh vacuum systems” *Appl. Opt.* **37**, 1762-1763 (1998).
- [33] M. Rosenblit, P. Horak, S. Hellsby, and R. Folman, “Single-atom detection using whispering-gallery modes of microdisk resonators” *Phys. Rev. A* **70**, 053808 (2004).
- [34] M. L. Gorodetsky, A. D. Pryamikov, and V. S. Ilchenko, “Rayleigh scattering in high-Q microspheres” *J. Opt. Soc. Am. B* **17**, 1051-1057 (2000).
- [35] T. J. Kippenberg, S. M. Spillane, and K. J. Vahala, “Modal coupling in traveling-wave resonators” *Opt. Lett.* **27**, 1669-1671 (2002).
- [36] C. W. Gardiner and M. J. Collett, “Input and output in damped quantum systems: Quantum stochastic differential equations and the master equation” *Phys. Rev. A* **31**, 3761-3774 (1985).
- [37] P. Domokos, M. Gangl, and H. Ritsch, “Single-atom detection in high-Q multimode cavities” *Opt. Comm.* **185**, 115-123 (2000).